

Synthesis and spectroscopic interpretations of Co(II), Ni(II) and Cu(II) decychole complexes with molecular docking of COVID-19 protease

Moamen S. Refat^{1*}, Safyah B. Bakare², Tariq A. Altalhi¹, Kehkashan Alam³,
Ghaferah H. Al-Hazmi⁴

¹Department of Chemistry, College of Science, Taif University, P.O. Box 11099, Taif 21944, Saudi Arabia

²Faculty of Education, Shaqra University, Al Muzahimiyah, Shaqra, Riyadh Province, P.O. Box 205, Zip Code 11972, Kingdom Saudi Arabia

³Department of Chemistry, Faculty of Science, Aligarh Muslim University, Aligarh, 202002, India

⁴Department of Chemistry, College of Science, Princess Nourah bint Abdulrahman University, Riyadh 11671, KSA

*Corresponding author: e-mail: msrefat@yahoo.com & moamen@tu.edu.sa

Co(II), Ni(II) and Cu(II) decychole complexes are interesting due to their biologically active and deliberate interest in the research due to their coordination properties. The microanalytical ‘elemental analysis’, molar conductivity, (infrared and Raman) spectroscopy, thermal analyses (TGA/DSC), UV-vis spectra, and ESR for copper(II) decychole complex investigations were performed in the structural assignments of Co(II), Ni(II) and Cu(II) decychole complexes. Reaction of the sodium decychole ligand (C₂₄H₃₉O₄Na) with three transition metal ions form the complexes of formulae, [M(C₂₄H₃₉O₄)₂(H₂O)₂] · xH₂O where M = Co(II), Ni(II) and Cu(II) where x = 2 for Cu(II) and x = 4 in case of M = Co(II) or Ni(II) metal ions. The FTIR spectra of the complexes show that decychole molecule is present as bidentate ligand. Molecular docking utilizing to additionally examine the interaction of COVID-19 (6LU7) with different complexes of decychole acid with Co(II), Ni(II) and Cu(II). Furthermore, in the case of Co(II) decychole complex, the probe is surrounded by amino residues Met235, Pro241, Glu240, Pro108, Gln110, Phe294, and Ile152. The probe molecule of Ni(II) decychole complex is sited close to amino acids Tyr126, Tyr239, Leu287, Leu272, and Lys137. For, Cu(II) decychole complex, the residues of amino acids comprise of Pro132, Pro108, Gln110, Gly109, Ile200, Asn203, Val202, His246, Pro293 and Tyr154. The binding energy was determined from the docking reads for Co(II)–6LU7, Ni(II)–6LU7 and Cu(II)–6LU7 decychole compounds were found to be –446.99, –500.52, –398.13 kcal mol^{–1} individually.

Keywords: decychole acid; complexes; ESR; TGA/DSC; molecular docking.

INTRODUCTION

Decychole acid, commonly known as choline acid, and bile acid. Decychole acid is a secondary bile acid, which is byproducts of intestinal bacteria. The two primary bile acids secreted by the liver are cholic acid and chenodeoxychole acid. Decychole acid is soluble in alcohol and acetic acid. When it is pure, it comes in the form of a white to yellowish-white crystalline powder¹. Decychole acid has been used since its discovery in various fields of human medicine. Decychole acid is used in the human body to emulsify fats for absorption in the intestine. It is licensed in some countries as an emulsifier in the food industry². It is used outside the body to prevent and dissolve gallstones. Decychole acid is used in research as a mild detergent to isolate membrane-bound proteins³. Sodium decychole is often used as a biological cleanser to leach cells and dissolve cellular and membrane components⁴. Sodium decychole mixed with phosphatidylcholine, is used in mesotherapy injection to produce lipolysis, and has been used as an alternative to surgical excision in treating lipomas. Decycholes and bile acid derivatives, in general, are actively being studied as structures for inclusion in nanotechnology. They also found applications in microprinting as photoresist ingredients⁵. Some publications indicate the effect of decychole acid as an immunostimulant^{6, 7} of the innate immune system, activating the main actors, macrophages. According to these publications, enough decychole acid in the human body corresponds to a good immune reaction of the nonspecific immune system.

The carboxylic group is capable to interaction with different metal ions which can have a synergistic or antagonistic effect on the anti-microbial activity. It was found that anti-inflammatory and anti-bacterial activity of metal complexes was higher than that of the parent carboxylic acids⁸. The carboxylate group as a substituent serves as a site to a complex targeting group that can aid in the delivery of the compound to bacteria cells in the body⁹. The design and synthesis of transition metal complexes with carboxylic bonds have received much attention in coordination chemistry because this type of complex has potential applications in molecular magnets, catalysis, and supramolecular chemistry and biological systems^{10, 11}. The carboxylate anion can adopt a wide range of bonding modes (monodentate symmetric and asymmetric chelating and bidentate and monodentate bridging)¹². The literature survey of the past few years reveals the fact that a significant development in the field of biological activity of metal chelates plays a vital role in the case and treatment of cancer^{13–16}. Metal complexes of carboxylic acids have been studied extensively^{17, 18}, but there are not any works on complexes of decychole acid. A clear understanding of the structure and spectroscopic properties of metal complexes usable for their biological applications is the aim of the present work. The present work deals with the synthesis and characterization of Co, Ni, and Cu(II) complexes of decychole acid. Also, we aimed to study the interaction of COVID-19 protease (6LU7) by molecular docking studies, with all three complexes of decychole acid. Molecular docking was performed to determine the binding sites and binding energy. From this study, we can obtain the difference in the inhibitory effect of COVID-19 protease for the biological process.

EXPERIMENTAL

Chemicals

Sodium deoxycholate and metal salts ($\text{CoCl}_2 \cdot 6\text{H}_2\text{O}$, $\text{NiCl}_2 \cdot 6\text{H}_2\text{O}$, and $\text{CuCl}_2 \cdot 2\text{H}_2\text{O}$) were received from “Sigma–Aldrich Chemical Corporation, St. Louis, Mo, USA”.

Synthesis of deoxycholate complexes

Co, Ni, and Cu(II) complexes of deoxycholate complexes were prepared by the same procedures, methanol 95% was employed as solvent. All the chemical reagents were of analytical grade and used without further purifications. $\text{CoCl}_2 \cdot 6\text{H}_2\text{O}$, $\text{NiCl}_2 \cdot 6\text{H}_2\text{O}$, and $\text{CuCl}_2 \cdot 2\text{H}_2\text{O}$ (1 mmol) were dissolved in 20 mL of methanol and then these solutions were slowly added to 30 mL of an aqueous solution with 2 mmol of sodium deoxycholate under a magnetic stirring. The reaction mixtures were refluxed at 65°C for two hours and left stand to evaporate slowly at room temperature overnight. The obtained solid precipitates were filtered off, wash with hot methanol solvent, dried at 80°C and then stored under vacuum over anhydrous phosphorus pentoxide.

Instrumentals

The carbon, hydrogen and nitrogen elements have been performed using Perkin Elmer CHN 2400. The determination of the percentages of metal ions was estimated based on the thermal gravimetric analysis technique. Melting points were carried out using MPS10–120 Melting point apparatus. FTIR spectra of the synthesized complexes were performed on Bruker FTIR Spectrophotometer. At room temperature with freshly prepared solutions, molar conductance of 10^{-3} M solutions in dimethyl sulfoxide (DMSO) solvent were measured using a Jenway 4010 conductivity meter. The electronic spectra were scanned *in situ* dimethyl sulfoxide within 200–800 nm range by UV2 Unicam UV/Vis Spectrophotometer. The effective magnetic moment (μ_{eff}) of the complexes was measured using Gouy’s method by the help of a magnetic susceptibility balance from Johnson Metthey and Sherwood model. The ESR spectrum of the diamagnetic

copper(II) complex was scanned by a JES-FE2XG EPR-Spectrometer. Thermogravimetric analysis (TGA) experiments were measured using TGA/DSC–50H Shimadzu analyzer. All experiments were performed using a single loose top-loading platinum sample pan under nitrogen atmosphere at a flow rate of 30 mL/min and a 10°C/min heating rate for the temperature range 25–800°C.

Molecular docking

Molecular docking has been used to understand the best binding site of the synthesized metal complexes with the COVID-19 protease (6LU7) using the HEX 8.0 program¹⁹. The structure of the COVID-19 protease was downloaded from the online protein data bank (<http://www.rcsb.org>) in the pdb format¹⁹. The 3D structure of Co (II), Ni (II) and Cu (II) complexes was designed utilizing the Chem3D software. Avogadro version 1.2 was utilized for the optimization of the structure. The docked conformations were visualized utilizing the Discovery Studio¹⁹ or Chimera of the complex.

RESULTS AND DISCUSSION

Elemental analysis and conductance data

Analytical data of the Co, Ni, and Cu(II) deoxycholate complexes are summarized above in Table 1, and the results obtained are reliable with those calculated for the proposed formulae. All these complexes were stable at atmospheric conditions, non-hygroscopic, and soluble in organic solvents such as dimethyl sulfoxide (DMSO) and dimethyl formamide (DMF). The molar conductivity of the deoxycholate complexes in dimethyl sulfoxide (10^{-3} M) at 25°C is proportionate with their non-electrolytic nature ($15\text{--}20 \Omega^{-1} \text{cm}^2 \text{mol}^{-1}$)¹⁹. However, the analytical, spectroscopic, and magnetic data do enable us to predict the possible structure of the synthesized complexes.

The infrared band assignments of sodium deoxycholate salt and its Co(II), Ni(II), and Cu(II) deoxycholate complexes are tabulated in Table 2. To identify the coordination modes of the carboxylato group, the

Table 1. Microanalytical and physical analysis results for deoxycholate complexes

Compounds	Color	Yield/ (%)	Conductance/ $\Omega^{-1} \text{cm}^2 \text{mol}^{-1}$	Analysis Found/(Calcd) %		
				C	H	M
$[\text{Co}(\text{C}_{24}\text{H}_{39}\text{O}_4)_2(\text{H}_2\text{O})_2] \cdot 4\text{H}_2\text{O}$ Mwt = 950.17 g/mol	Red	65	20	60.54 (60.68)	9.43 (9.55)	6.09 (6.20)
$[\text{Ni}(\text{C}_{24}\text{H}_{39}\text{O}_4)_2(\text{H}_2\text{O})_2] \cdot 4\text{H}_2\text{O}$ Mwt = 949.93 g/mol	Green	68	15	60.33 (60.69)	9.21 (9.55)	6.11 (6.18)
$[\text{Cu}(\text{C}_{24}\text{H}_{39}\text{O}_4)_2(\text{H}_2\text{O})_2] \cdot 2\text{H}_2\text{O}$ Mwt = 918.75 g/mol	Green	71	18	62.70 (62.75)	9.39 (9.44)	6.88 (6.92)

Table 2. Infrared spectral assignments of the deoxycholate complexes

Sodium deoxycholate	Co(II)	Ni(II)	Cu(II)	Assignments
3394	3373	3387	3415	ν (OH)
2935	2933	2933	2934	ν_{as} (CH)
2864	2862	2864	2864	ν_{s} (CH)
1566	1552	1542	1596	ν_{as} (OCO)
1449, 1406, 1302	1461, 1410, 1332, 1299	1420, 1376, 1301	1448, 1417, 1377, 1304	δ (CH ₂) + ν_{s} (OCO)
1164	1206	1164	1165	ρ_{w} (CH ₂)
1093, 1040	1093, 1041	1091, 1039	1090, 1038	ν_{as} (CC)
945	946	944	945	ν_{s} (CC)
917	849, 805	850, 789	851	δ (CC) + δ (OCO)
614	656, 615	710, 614	652, 615	ρ_{w} (OCO) + ν (M-O)

difference between the asymmetric and symmetric carboxylate vibrations ($\Delta\nu = \nu_{\text{asym}} - \nu_{\text{sym}}$) was calculated. The carboxylate group acts as a monodentate manner, when the difference between the $\nu_{\text{asCOO}} - \nu_{\text{sCOO}}$ is larger than ionic compounds^{19, 20}. When the $\Delta\nu$ is considerably smaller than the ionic compound, the carboxylate group coordinated towards metal ions as a bidentate fashion. In the spectra of the deoxycholate sodium salt and complexes, characteristic infrared bands arising from the frequencies of the carboxylate anion appeared. The stretching vibrations of the symmetric carboxylate anion $\nu_{\text{sym}}(\text{COO})$ are present at the wavenumbers 1566 cm^{-1} , 1552 cm^{-1} , 1542 cm^{-1} , and 1596 cm^{-1} in deoxycholate sodium salt,²⁰ cobalt complex, nickel complex, and copper complex respectively, and the stretching asymmetric $\nu_{\text{as}}(\text{COO})$ at the wavenumbers 1302 cm^{-1} , 1332 cm^{-1} , 1376 cm^{-1} , and 1377 cm^{-1} IR in deoxycholate sodium salt, cobalt complex, nickel complex, and copper complex respectively (Table 3). Based on the position of the ν_{asCOO} and ν_{sCOO} bands in the IR spectra of the synthesized complexes compared to the position of these bands in the sodium salt, it was found that the differences between the frequencies were determined as 264, 220, 166 and 219 for deoxycholate sodium salt, cobalt complex, nickel complex, and copper complex respectively. These results for Δ values indicated that the carboxylate group participates in a bidentate manner for the complexes (Fig. 1).

New vibration bands have been noticed in spectra of prepared complexes at wave number ranges 615 cm^{-1} assigned to $\nu(\text{M-O})$ vibrations²⁰.

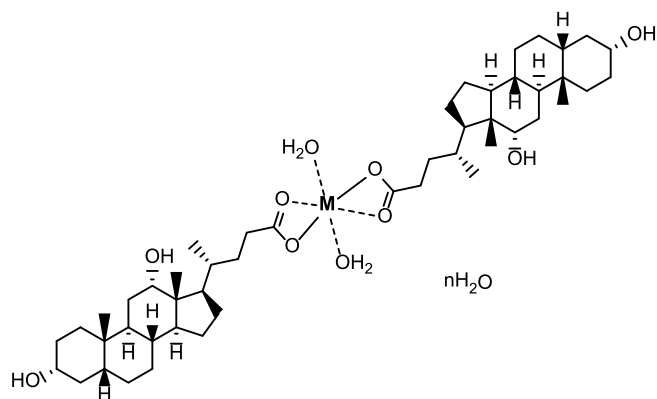


Figure 1. Proposed structures of deoxycholate complexes (where $n = 4$ for Co(II) and Ni(II) complexes; $n = 2$ for Cu(II) complex)

UV-Vis spectra, ESR and magnetic susceptibility

The electronic reflectance spectra of Co(II), Ni(II), and Cu(II) deoxycholate complexes were recorded in solid-state. The octahedral cobalt(II) complexes have a pink or reddish brown²¹ but most tetrahedral Co(II) complexes have an intense blue or green color, herein the electronic spectrum of the red color complex, [Co-

$(\text{C}_{24}\text{H}_{39}\text{O}_4)_2(\text{H}_2\text{O})_2] \cdot 4\text{H}_2\text{O}$, showed that this complex has an octahedral geometry. There are two electronic bands at 23529 cm^{-1} and 28571 cm^{-1} attributed to ${}^4\text{T}_{1g} \rightarrow {}^4\text{A}_{2g}$ and ${}^4\text{T}_{1g} \rightarrow {}^4\text{T}_{1g}(\text{P})$ transitions, respectively. The magnetic moment of the cobalt(II) complex was found at 3.84 B.M. at room temperature which supported the octahedral geometry (Fig. 1). The electronic spectra of the synthesized nickel(II) exhibited two electronic absorption bands at 14970 and 29239 cm^{-1} correspond to the ${}^3\text{A}_{2g}(\text{F}) \rightarrow {}^3\text{T}_{1g}(\text{F})$ (ν_2) and ${}^3\text{A}_{2g}(\text{F}) \rightarrow {}^3\text{T}_{1g}(\text{P})$ (ν_2) transitions respectively. These transitions revealed that the nickel(II) complex has an octahedral geometry²². The effective magnetic moment value (μ_{eff}) of the Ni(II) complex was 3.20 BM. This value indicated that there were two unpaired electrons so that the complex was paramagnetic. The values of μ_{eff} 3.20 BM in the nickel complex indicated an octahedral complex²³. Hence, the Ni(II) complex was suspected to have octahedral geometry. The electronic spectrum of the green copper(II) complex, $[\text{Cu}(\text{C}_{24}\text{H}_{39}\text{O}_4)_2(\text{H}_2\text{O})_2] \cdot 2\text{H}_2\text{O}$ (Fig. 1) showed distinguish transition band at 20121 cm^{-1} ascribe to ${}^2\text{E}_g \rightarrow {}^2\text{T}_{2g}$ transition in a distorted octahedral geometry²¹. The other absorption band at 28329 cm^{-1} was assigned to L→M charge transfer. The found value of the magnetic moment of Cu(II) complex was 1.76 B.M., which supported the octahedral feature²¹.

X-band ESR spectrum of copper(II) complex, $[\text{Cu}(\text{C}_{24}\text{H}_{39}\text{O}_4)_2(\text{H}_2\text{O})_2] \cdot 2\text{H}_2\text{O}$ exhibited axial patterns of four lines due to the hyperfine coupling of the unpaired electrons with the copper nucleus (${}^{63}\text{Cu}$, $I = 3/2$). The g and A values were calculated from the spectrum of the Cu(II) complex (Fig. 2). The trend $g_{\parallel} (2.1294) > g_{\perp} (1.5971)$ observed in copper(II) complex indicate that the Cu(II) is in a distorted octahedral coordination environment, and the unpaired electron most likely resides predominantly in the $d_{x^2-y^2}$ orbital of the Cu(II) ion and is the characteristic feature for the axial symmetry. The deviation of “ g ” values from the free-electron value (2.0023) is by angular momentum contribution in the complexes. The average “ g ” value for overall distortion is calculated using the equation: $g_{\text{av}} (1.7745) = 1/3(2g_{\perp} + g_{\parallel})$ ²⁴. Molecular orbital coefficients in-plane σ -bonding (α^2), in-plane π -bonding (β^2), and out-of-plane π -bonding (γ^2) are the covalency parameters for the metal to ligand bond which were evaluated using the following expressions:

$$\alpha^2 = (A_{\parallel}/0.036) + (g_{\parallel} - 2.0027) + 3/7 (g_{\perp} - 2.0023) + 0.04$$

$$\beta^2 = (g_{\parallel} - 2.0023)E / -8\lambda\alpha^2$$

$$\gamma^2 = (g_{\parallel} - 2.0023)E / -2\lambda\alpha^2$$

where $\lambda = -829 \text{ cm}^{-1}$ for the free copper ion and E is the electronic transition energy. The observed values of α^2 and β^2 indicate that the complex has covalent bonding character. The smaller the β^2 , the larger the covalency of the bonding. Furthermore, it has appeared that the covalency of the out-of-plane is greater than of the in-plane π -bonding.

Table 3. The stretching of asymmetric and symmetric vibrations of the carboxylate group

Compounds	$\nu_{\text{as}}(\text{COO})$	$\nu_{\text{s}}(\text{COO})$	$\Delta\nu = \nu_{\text{as}} - \nu_{\text{s}}$	Bonding mode
sodium deoxycholate	1566	1302	264	ionic
Co(II)	1552	1332	220	Bidentate
Ni(II)	1542	1376	166	Bidentate
Cu(II)	1596	1377	219	Bidentate

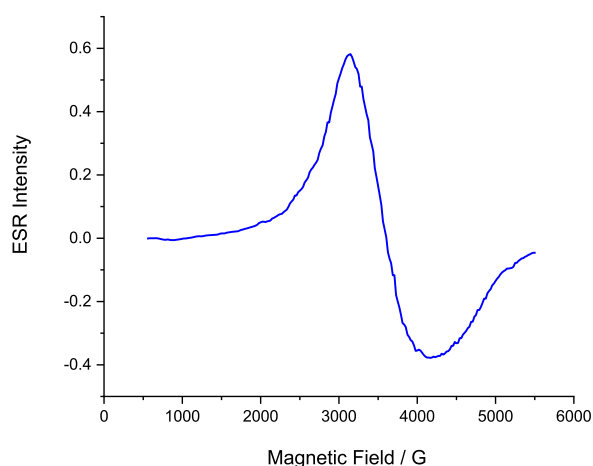


Figure 2. ESR spectrum of copper (II) deoxycholate complex

Thermal analysis

The TG/DSC study for the $[\text{Co}(\text{C}_{24}\text{H}_{39}\text{O}_4)_2(\text{H}_2\text{O})_2] \cdot 4\text{H}_2\text{O}$, $[\text{Ni}(\text{C}_{24}\text{H}_{39}\text{O}_4)_2(\text{H}_2\text{O})_2] \cdot 4\text{H}_2\text{O}$ and $[\text{Cu}(\text{C}_{24}\text{H}_{39}\text{O}_4)_2(\text{H}_2\text{O})_2] \cdot 2\text{H}_2\text{O}$ deoxycholate complexes are assigned and listed in Table 4 and the thermal diagrams are shown in Fig. 3a–c. The final solid products as a residual that is associated with the thermal decompositions of deoxycholate complexes are CoO, NiO and CuO.

The TGA/DSC curves of the cobalt(II) complex show four endothermic peaks at (71, 428, 496, and 621°C) and three exothermic peaks at (710, 745, and 771°C) with a total mass loss 93% (calcd. 92.11%) corresponds to the release of two deoxycholate ($\text{C}_{24}\text{H}_{39}\text{O}_4$), six coordinated and uncoordinated water molecules. Hence, the cobalt(II) deoxycholate complex decomposes to cobalt oxide (CoO) with intermediate formation of cobalt carbonate (see Fig. 3a). The two $[\text{Ni}(\text{C}_{24}\text{H}_{39}\text{O}_4)_2(\text{H}_2\text{O})_2] \cdot 4\text{H}_2\text{O}$ and $[\text{Cu}(\text{C}_{24}\text{H}_{39}\text{O}_4)_2(\text{H}_2\text{O})_2] \cdot 2\text{H}_2\text{O}$ deoxycholate complexes are stable up to 100°C with DSC maximum peaks at (110°C, 320°C, 498°C, and 690°C) and (100°C, 327°C, 430°C, and 585°C) respectively, and then lose the two deoxycholate molecules in three decomposition steps (Figs. 3b&c) over 100–700°C. The anhydrous two complexes decompose to metal carbonate form as an intermediate over 300°C and the last one with the formation of NiO and CoO oxides.

It is evident that different complexes of sodium deoxycholate with Co(II), Ni(II) and Cu(II) may have a unique impact on COVID-19 protease. However, it is hard to decide the differences through the experiments. Henceforth, to determine the difference, a computational study could be utilized^{25, 26}. So, the molecular docking was performed

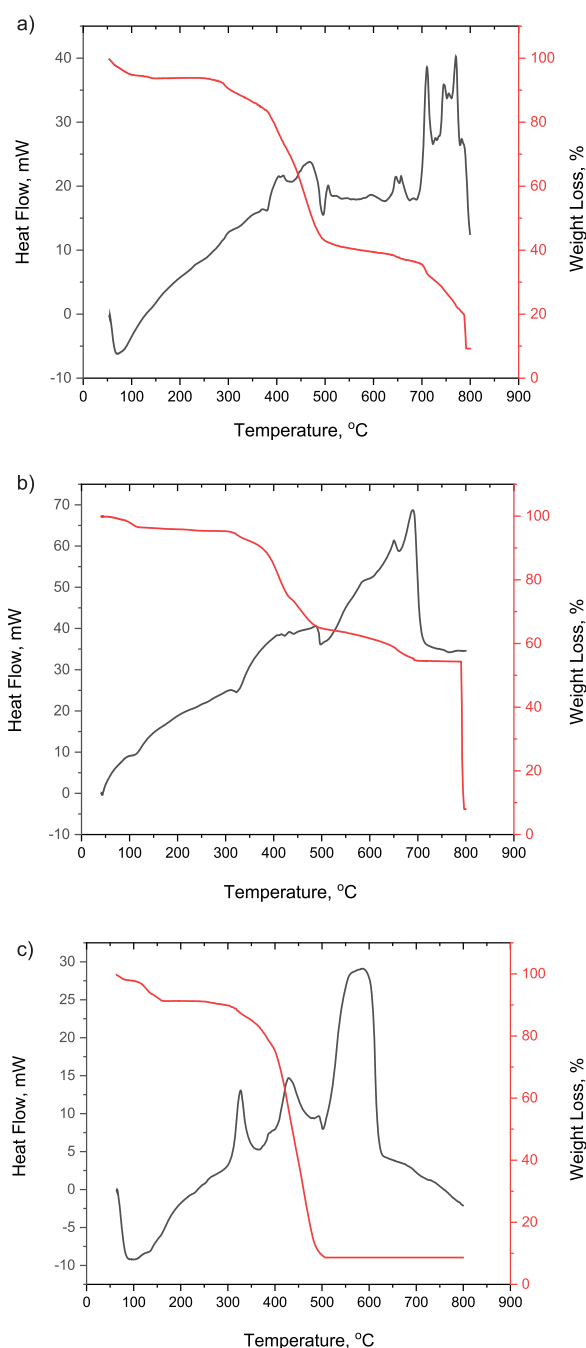


Figure 3. a) TGA and DSC curves of $[\text{Co}(\text{C}_{24}\text{H}_{39}\text{O}_4)_2(\text{H}_2\text{O})_2] \cdot 4\text{H}_2\text{O}$ complex; b) TGA and DSC curves of $[\text{Ni}(\text{C}_{24}\text{H}_{39}\text{O}_4)_2(\text{H}_2\text{O})_2] \cdot 4\text{H}_2\text{O}$ complex; c) TGA and DSC curves of $[\text{Cu}(\text{C}_{24}\text{H}_{39}\text{O}_4)_2(\text{H}_2\text{O})_2] \cdot 2\text{H}_2\text{O}$ complex

Table 4. Main TGA and DSC data for the deoxycholate complexes

Complexes	DSC T/°C peak	TG data			
		T range (°C)	Mass loss (%) Found (Calc.)	Losses molecules	Residue products
$[\text{Co}(\text{C}_{24}\text{H}_{39}\text{O}_4)_2(\text{H}_2\text{O})_2] \cdot 4\text{H}_2\text{O}$	71 endo 428 endo 496 endo 621 endo 710 exo 745 exo 771 exo	30–100 100–500 500–600 600–700 700–730 730–760 760–800	93(92.11)	$2(\text{C}_{24}\text{H}_{39}\text{O}_4)$ $6\text{H}_2\text{O}$	CoO
$[\text{Ni}(\text{C}_{24}\text{H}_{39}\text{O}_4)_2(\text{H}_2\text{O})_2] \cdot 4\text{H}_2\text{O}$	110 endo 320 endo 498 endo 690 exo	30–120 120–400 400–600 600–800	92.50(92.14)	$2(\text{C}_{24}\text{H}_{39}\text{O}_4)$ $6\text{H}_2\text{O}$	NiO
$[\text{Cu}(\text{C}_{24}\text{H}_{39}\text{O}_4)_2(\text{H}_2\text{O})_2] \cdot 2\text{H}_2\text{O}$	100 endo 320 endo 498 endo 690 exo	30–150 150–400 400–600 600–800	91(91.34)	$2(\text{C}_{24}\text{H}_{39}\text{O}_4)$ $4\text{H}_2\text{O}$	CuO

to identify the interaction of 6LU7 with Co(II), Ni (II) and Cu(II) deoxycholate complexes. The most possible docking pose between 6LU7 and different complexes of sodium deoxycholate and related data are shown in Table 5, 6 and Fig. 4–6. The binding sites of prepared complexes show that interactions are considerably different in each case as represented from Fig. 4–6. In the case of Co(II) deoxycholate complex, the probe molecule is bounded

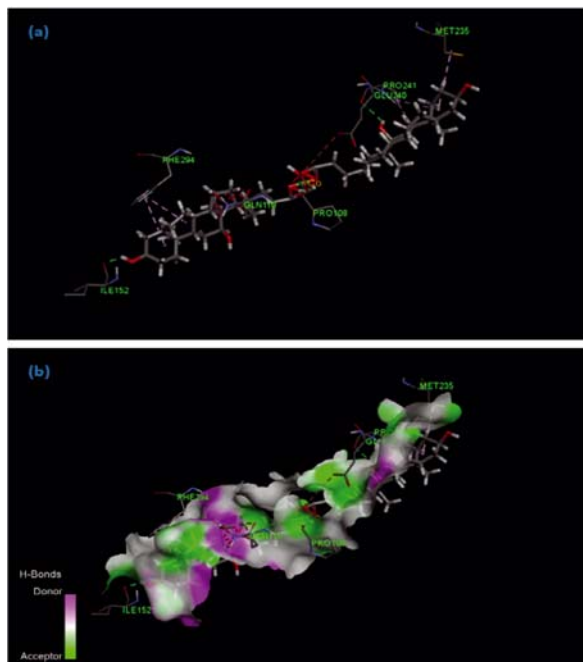


Figure 4. Molecular docking pose of the Co(II) complex with COVID-19 protease (6LU7) (a) Showing interaction with amino acids (b) surface showing hydrogen bond interaction

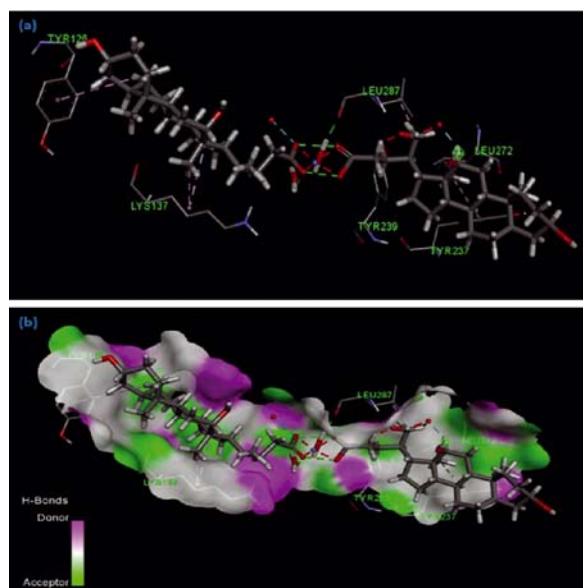


Figure 5. Molecular docking pose of the Ni (II) complex with COVID-19 protease (6LU7); (a) Showing interaction with amino acids; (b) surface showing hydrogen bond interaction

Table 5. The docking interactions parameters

Complexes	Binding free energy (kcal/mol)	Total Intermolecular energy (kcal/mol)	Interacting amino acids
Co(II)	- 446.99	- 3.45	Met235, Pro241, Glu240, Pro108, Gln110, Phe294, Ile152
Ni(II)	- 500.52	- 6.37	Tyr126, Tyr239, Leu287, Leu272, Lys137
Cu(II)	- 398.13	- 1.65	Pro132, Pro108, Gln110, Gly109, Ile200, Asn203, Val202, His246, Pro293, Tyr154

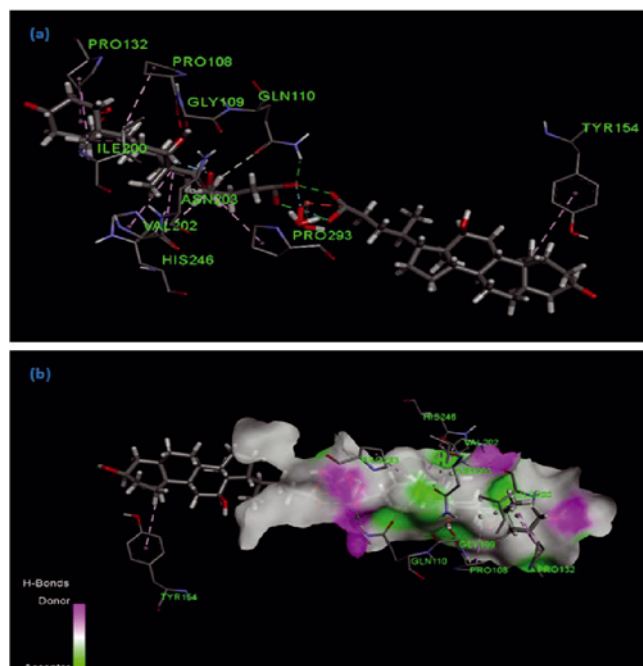


Figure 6. Molecular docking pose of the Cu(II) complex with COVID-19 protease (6LU7) (a) Showing interaction with amino acids (b) surface showing hydrogen bond interaction

by amino acid residues Met235, Pro241, Glu240, Pro108, Gln110, Phe294, Ile152. The probe molecule of Ni(II) deoxycholate complex is sited next to amino acid residues Tyr126, Tyr239, Leu287, Leu272, and Lys137. For, Cu(II) deoxycholate complex, the amino acid residue consists of Pro132, Pro108, Gln110, Gly109, Ile200, Asn203, Val202, His246, Pro293, Tyr154. In addition, four hydrogen bonds are observed in Co(II), Ni(II) complex while five hydrogen bonds are found in the case of Cu(II) deoxycholate complex and other details are summarized in Table 6. The value of binding energy was calculated from the docking studies for Co(II)-6LU7, Ni(II)-6LU7 and Cu(II)-6LU7 deoxycholate complexes were - 446.99, - 500.52, - 398.13 kcal mol⁻¹ respectively. The binding affinity of Co(II)-COVID-19 protease was found to be - 446.99 kcal mol⁻¹ indicating the slightly higher binding energy than Cu(II)-6LU7 and slightly lower than Ni(II)-6LU7. The estimated inhibition

Table 6. Hydrogen bond interactions

Complexes	Residue	Amino Acid	Distance H-A	A (Acceptor atom)
Co(II) deoxycholate complex	108A	Pro	2.11	O ₂
	110A	Gln	3.10	O ₃
	153A	Asp	3.20	O ₂
	241A	Pro	2.61	O ₂
Ni(II) deoxycholate complex	131A	Arg	3.44	O ₃
	131A	Arg	3.96	O ₃
	287A	Leu	2.97	O ₂
	289A	Asp	3.02	O ₂
Cu(II) deoxycholate complex	109A	Gly	2.56	O ₂
	110A	Gln	2.12	O ₃
	198A	Thr	2.45	O ₃
	292A	Thr	3.26	O ₃
	294A	Phe	1.62	O ₃

Constant, K_i is 48.39 mM (millimolar) which is found in the case of Cu(II) complex²⁷. So, this complex has a higher ability to inhibit the biological process of target COVID-19 protease (6LU7).

CONCLUSION

The synthesis of the complexes between sodium deoxycholate and essential metal ions (Co(II), Ni(II) and Cu(II)) were studied to investigate the complexation behavior of these systems as it could mimic many biological interactions. The complexes appear to be superior in biological properties dependent on the molecular docking that utilizing to additionally examine the interaction of COVID-19 (6LU7). The complete elucidation molecular structures of the synthesized deoxycholate complexes were confirmed by detailed microanalytical 'elemental analysis', molar conductivity, (infrared and Raman) spectroscopy, thermal analyses (TGA/DSC), UV-vis spectra, and ESR techniques. The spectroscopic analysis of the complexes shows that deoxycholate molecule acts as a bidentate ligand with octahedral geometry.

ACKNOWLEDGMENT

Taif University Researches Supporting Project number (TURSP-2020/01), Taif University, Taif, Saudi Arabia.

LITERATURE CITED

- Lide, D.R. (1998). *Handbook of Chem. and Physics.* (87 ed.). Boca Raton, FL: CRC Press. p. 1287.
- Streuli, H. (1992). SLMB – Schweizer Lebensmittelbuch, chapter 58, 4/3.
- Neugebauer, J.M. (1990). "Detergents: An Overview" in M.P. Deutscher, Guide to Protein Purification (Methods in Enzymology Vol. 182), Academic Press, San Diego. DOI: 10.1016/0076-6879(90)82020-3.
- Duncan, D. & Rotunda, A.M. (2011). Injectable therapies for localized fat loss: state of the art. *Clin. Plast Surg.*, 38(3), 489–501, DOI: 10.1016/j.cps.2011.02.005.
- Kim, J.B., Lee, B.W., Yun, H.J. & Kwon, Y.G. (2000). 193-nm Photoresists Based on Norbornene Copolymers with Derivatives of Bile Acid. *Chem. Lett.*, 29(4), 414–415. DOI: 10.1246/cl.2000.414.
- Vlček, B. (1972). Potentiation of the immune response with DCA (Czech). *Prakt. Lekar.*, 52, 326–30.
- Chyle, M. & Chyle, P. (1982). *Regulation of the immune response with DCA (Czech, engl. summary).* *Sborník lek.*, 84, 212–218.
- World Health Organisation International Programme on Chemical Safety, Concise International Chemical Assessment Document No. 26, Geneva, (2000).
- Chohan, Z.H. & Sherazi, S.K.A. (1997). Synthesis, characterization and role of anions (nitrate, sulphate, oxalate and acetate) in the biological activity of hydrazine derived compounds and their metal chelates. *Metal-Based Drugs*, 4, 327.
- Knapp, A.R., Panzner, M.J., Medvetz, D.A., Wright, B.D., Tessier, C.A. & Youngs, W.J. (2010). Synthesis and antimicrobial studies of silver N-heterocyclic carbene complexes bearing a methyl benzoate substituent. *Inorg. Chim. Acta*, 364(1), 125–131. DOI: 10.1016/j.ica.2010.08.008.
- Rardin, R.L., Tolman, W.B. & Lippard, S.J. (1991). Monodentate carboxylate complexes and the carboxylate shift: implications for polymetalloprotein structure and function. *New J. Chem.*, 15(6), 417–430.
- Holm, R.H., Kennepohl, P. & Solomon, E.I. (1996). Structural and Functional Aspects of Metal Sites in Biology. *Chem. Rev.*, 96(7), 2239–2314. DOI: 10.1021/cr9500390.
- Busch, D.H. & Stephenson, N.A. (1990). Molecular organization, portal to supramolecular chemistry: Structural analysis of the factors associated with molecular organization in coordination and inclusion chemistry, including the coordination template effect. *Coord. Chem. Rev.*, 100, 119–154. DOI:10.1016/0010-8545(90)85007-F.
- Rosenberg, B., Vancamp, L., Trosko, J.E. & Mansour, V.H. (1969). Platinum Compounds: a New Class of Potent Antitumour Agents. *Nature*, 222, 385–386. DOI: 10.1038/222385a0.
- Canali, L. & Sherrington, D.C. (1999). Utilisation of homogeneous and supported chiral metal(salen) complexes in asymmetric catalysis. *Chem. Soc. Rev.*, 28, 85–93. DOI: 10.1039/A806483K.
- Tejam, A.B. & Thakkar, N. (1997). Extractive spectrophotometric determination of Co(II) at trace level using l-phenyl 1,2-propanedione dioxime. *Indian J. Chem.*, 36(A), 1008–1009.
- Bhai, S. & Ganguly, B. (2019). Role of backbones on the interaction of metal ions with deoxyribonucleic acid and peptide nucleic acid: A DFT study. *J. Mol. Graph. Model.*, 93, 107445. DOI: 10.1016/j.jmgm.2019.107445.
- Murphy, J.M., Powell, B.A. & Brumaghim, J.L. (2020). Stability constants of bio-relevant, redox-active metals with amino acids: The challenges of weakly binding ligands. *Coord. Chem. Rev.*, 412, 213253. DOI: 10.1016/j.ccr.2020.213253.
- Deacon, G.B. & Phillips, R.J. (1980). Relationships between the carbon-oxygen stretching frequencies of carboxylate complexes and the type of carboxylate coordination. *Coord. Chem. Rev.*, 33, 227–250. DOI: 10.1016/S0010-8545(00)80455-5.
- Khan, I.M., Alam, K., Alam, M.J. & Ahmad, M. (2019). Spectrophotometric and photocatalytic studies of H-bonded charge transfer complex of oxalic acid with imidazole: single crystal XRD, experimental and DFT/TD-DFT studies. *New J. Chem.*, 43, 9039–9051. DOI: 10.1039/C9NJ00332K.
- Nakamoto, K. (1997). *Infrared and Raman Spectra of Inorganic and Coordination Compounds*, Wiley, New York.
- Lever, A.B.P. (1997). *Inorganic Electronic Spectroscopy*, 2nd ed., Elsevier, Amsterdam.
- Craig, G.A., Sarkar, A., Woodall, C.H., Hay, M.A., Marriot, K.E., Kamenev, K.V., Moggach, S.A., Brechin, E.K., Parsons, S., Rajaraman, G. & Murrie, M. (2018). Probing the origin of the giant magnetic anisotropy in trigonal bipyramidal Ni(II) under high pressure. *Chem. Sci.*, 9, 1551–1559. DOI: 10.1039/C7SC04460G.
- Omaka, N.O., Ekennia, A.C., Njoku, N.N. & Onwudiwe, D.C. (2018). Nickel(II) and copper(II) complexes of 2,2'-bibenzo[d]thiazole: Synthesis, characterisation and biological studies. *App. Organomet. Chem.*, 32(4), e4241. DOI: 10.1002/aoc.4241.
- Yernale, N.G. & Mruthyunjayaswamy, B.H.M. (2014). Synthesis, Characterization, Antimicrobial, DNA Cleavage, and In Vitro Cytotoxic Studies of Some Metal Complexes of Schiff Base Ligand Derived from Thiazole and Quinoline Moiety. *Bioinorg. Chem. Appl.*, 2014, Article ID 314963, 17. DOI: 10.1155/2014/314963.
- Zhang, F., Zhang, J., Tong, C.L., Chen, Y.D., Zhuang, S.L. & Liu, W.P. (2013). Molecular interactions of benzophenone UV filters with human serum albumin revealed by spectroscopic techniques and molecular modeling. *J. Hazard. Mater.*, 263, 618–626. DOI: 10.1016/j.jhazmat.2013.10.024.
- Elgawish, M.S., Kishikawa, N., Helal, M.A., Ohyama, K. & Kuroda, N. (2015). Molecular modeling and spectroscopic study of quinone-protein adducts: insight into toxicity, selectivity, and reversibility. *Toxicol. Res.*, 4, 843–847. DOI: 10.1039/c5tx00098j.
- Mumit, M.A., Pal, T.K., Alam, M.A., Islam, M.A., Paul, S. & Sheikh, M.C. (2020). DFT studies on vibrational and electronic spectra, HOMO–LUMO, MEP, HOMA, NBO and molecular docking analysis of benzyl-3-N-(2,4,5-trimethoxyphenylmethylene)hydrazinecarbodithioate. *J. Mol. Struct.*, 1220, 128715. DOI: 10.1016/j.molstruc.2020.128715.